RevLock: A Reversible Self-Locking Mechanism Driven by Linear Actuators for Foldable Robots and Systems

A. Fernandes Minori, U. Civici, C. Shen, S. Paul, S. Bergbreiter, Z. Temel, and L. Yao

***Abstract*—The designs of origami-and kirigami-inspired robots enable configurations from 2D to 3D shapes, lightweight systems, and take advantage of rapid fabrication techniques. These features have been explored for robotics in applications ranging from aerospace to medical devices. However, achieving reversible reconfigurations that sustain/lock between shapes without requiring constant energy input and allow system integration (e.g., sensing, assembly) is challenging. This letter proposes a design and fabrication approach that uses electrically driven mechanisms to enable reversible self-reconfiguration and locking without constant energy input. We leverage origami and kirigami-inspired designs to transmit the motions of a planar artificial muscle and low melting point alloys for time-controlled locking. Using these techniques, we demonstrate compact systems in multiple reconfigurable robotic applications, from gripping to crawling.**

***Index Terms*—Actuation and joint mechanisms, foldable robots, soft robot materials and design, soft robot applications.**

Manuscript received 21 April 2023; accepted 23 August 2023. Date of publication 15 September 2023; date of current version 4 October 2023. This letter was recommended for publication by Associate Editor S. Song and Editor Y.-L. Park upon evaluation of the reviewers' comments. This work was supported by the NSF under Grants CNS-2127309 and IIS-CAREER-2047912. *(C. Shen and S. Paul contributed equally to this work.) (Corresponding authors: A. Fernandes Minori; S. Bergbreiter; L. Yao.)*

A. Fernandes Minori is with the School of Computer Science, Human-Computer Interaction Institute, Carnegie Mellon University, Pittsburgh, PA 15213 USA, and also with the Department of Mechanical Engineering, Carnegie Mellon University, Pittsburgh, PA 15213 USA (e-mail: aminori@andrew.cmu.edu).

U. Civici is with the School of Computer Science, Human-Computer Interaction Institute, Carnegie Mellon University, Pittsburgh, PA 15213 USA, and also with the School of Engineering and Applied Sciences, Harvard University, Cambridge, MA 02138 USA (e-mail: umutcivici@seas.harvard.edu).

C. Shen is with the School of Computer Science, Human-Computer Interaction Institute, Carnegie Mellon University, Pittsburgh, PA 15213 USA, and also with the School of Architecture, Carnegie Mellon University, Pittsburgh, PA 15213 USA (e-mail: chenyis@andrew.cmu.edu).

S. Paul is with the Department of Mechanical Engineering, University of California Santa Barbara, Santa Barbara, CA 93106 USA (e-mail: s_paul@ucsb.edu).

S. Bergbreiter is with the Department of Mechanical Engineering, Carnegie Mellon University, Pittsburgh, PA 15213 USA (e-mail: sbergbre@andrew.cmu.edu).

Z. Temel is with the School of Computer Science, Robotics Institute, Carnegie Mellon University, Pittsburgh, PA 15213 USA (e-mail: ztemel@cs.cmu.edu).

L. Yao is with the School of Computer Science, Human-Computer Interaction Institute, Carnegie Mellon University, Pittsburgh, PA 15213 USA (e-mail: liningy@andrew.cmu.edu).

This letter has supplementary downloadable material available at https://doi.org/10.1109/LRA.2023.3315215, provided by the authors.

Digital Object Identifier 10.1109/LRA.2023.3315215

I. Introduction

RECONFIGURABLE robotics have the ability to change shape to achieve a task or multiple tasks [1], [2]. Origami (i.e., the art of folding) and kirigami (i.e., the art of cutting and folding) are two especially attractive design paradigms for these reconfigurable robots because they enable systems that are lightweight, compliant, and can be reconfigured from 2D to 3D shapes. The monolithic fabrication approaches used in origami and kirigami robots can be batch fabricated within a few hours while also enabling circuits, actuation, and sensing within the same process [3]. Examples of robotic systems that take advantage of origami and kirigami span applications such as ingestible robotics [2], robotic arms [4], and telerobotics [5], [6].

An essential component of engineering these morphing robots is the ability to lock between shapes. Deployable robots often need to maintain a compact shape until they are deployed as more expansive robotic systems [7], and reconfigurable robots can reversibly change their shape depending on the task [8]. However, achieving these reconfigurations, especially for origami and kirigami robotics, without adding additional design constraints (e.g., weight, constant energy input, size) is still challenging. Previous work has explored actuation and locking strategies that either: i) take advantage of bulky external power sources or circuitry [3], [9]; ii) use responsive materials that are not reversible once the stimuli cease, limiting their ability to reconfigure [3], [7]; or iii) are challenging to integrate with other components (either in fabrication or for sensing and control [10], [11]). Some of these approaches are summarized in Table I.

Both passive and active locking strategies have been previously studied for general (i.e., not limited to origami/kirigami) reconfigurable robots. Some passive locking strategies that do not require additional energy input include magnetic locking [16], mechanical locking [4], antagonistic actuation [17], and multistable mechanisms [12], [18], [19]. However, these locking strategies either require additional actuation, control strategies (e.g., undesired proximity locking/unlocking), or intricate design constraints (e.g., locking under a specific range of geometries for the same material, or compromising the strength-to-weight ratio). These challenges can limit the design and fabrication landscape due to additional complexity of mechanical design and system integration, leading to significant challenges in system integration with origami and kirigami robotics.

In contrast, active locking strategies for reconfigurable robots have taken advantage of electromagnetic actuation [8], [15], fluidic systems [20], [21], or smart materials (e.g., shape-memory

TABLE I
COMPARISON OF REVERSIBLE SELF-LOCKING DESIGNS; "-" INDICATES THAT DATA IS NOT REPORTED OR APPLICABLE, $^*E_c = P_{lock} * t_{lock} + P_{unlock} * t_{unlock}$

Design Type	Locking Material	Locking Size (mm)	Assembly Method	Strength-to-Weight Ratio	Total Energy Consumed (Ec)* For Locking and Unlocking (J)
Origami/Kirigami [4]	Magnets and Geometry	40 x 100 x 16	Wiring	**545**	-
Origami/Kirigami [12]	Bistability	12 x 20 x 0.5	Wiring	150	-
Origami/Kirigami (**RevLock**)	LMPA	**4 x 3 x 1.5**	**Monolithic**	**266**	**66**
3D printed [13]	LMPA	30 x 30 x 0.8	**Monolithic**	147	140
3D printed [14]	SMP	70 x 60 x 7	Wiring/Gluing	-	450
3D printed [15]	Electro Perm. Magnets	**5.9 x 2.5 x 1.3**	**Monolithic**	17.4	**0.03**

polymers, SMPs [3]). The advantages of these active locking strategies include easy access to parts and control policies. Smart materials also provide a straightforward fabrication approach that can be more easily integrated with origami and kirigami robots. However, these actuation methods often require constant energy input, exceptionally high electrical input (e.g., power, current/voltage), or device control to lock between shapes.

These requirements add bulky external components (e.g., circuitry integration and size) that hinder portability, noise, or reversibility between shapes once the stimulus stops. Furthermore, their material properties (e.g. glass transition temperature), and strength-to-weight ratio can limit their applicability, particularly for those materials that are not reversible once the stimuli cease [3], [14]. Low melting point alloys (LMPAs) are another emerging material used for locking. They can melt and self-fuse with each other when they are above their transition temperature, and they can solidify to mechanically lock when they are cooled below it. Energy input is only required for the transition. They have previously been used in more general reconfigurable robotics [13] and shape-programmable soft robots [17], [22] that take advantage of compact integration and lightweight LMPAs. However, LMPAs have not previously been integrated into fabrication and design approaches for origami and kirigami robots, as seen in Table I.

In this work, we seek to combine origami/kirigami techniques together with LMPA to leverage the benefits of active and passive locking. We propose a design and fabrication framework (RevLock) to achieve compact, reversible self-locking Origami/Kirigami robotic systems without constant energy input and with a single linear actuator. The first contribution of this work is to electrically fuse and un-fuse multilayer laminate mechanisms by combining laminate fabrication techniques with LMPA droplets. While liquid crystal elastomers (LCEs) are used as linear actuators in this work to bring LMPA droplets into contact, our method is designed to work with any linear actuators that are compatible with origami and kirigami fabrication and design. Finally, we leverage the advantages of this hybrid assembly (i.e., active and passive layers with rigid and flexible materials) to demonstrate lightweight reconfigurable robotic systems, including a crawler and a gripper (Fig. 1). (A glider is presented in the Supp. Video only).

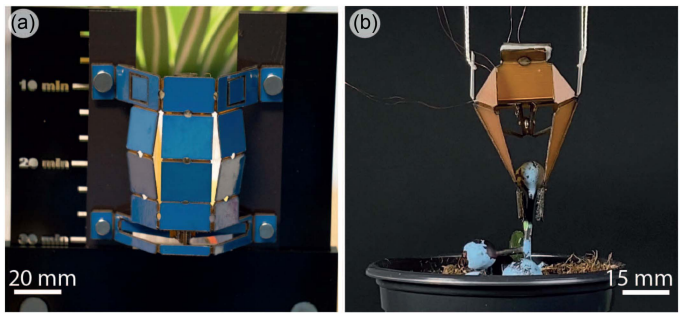

Fig. 1. Examples of foldable robots and systems using the Revlock concept: (a) a self-assembled crawling robot, and (b) a gripper for timed delivery.

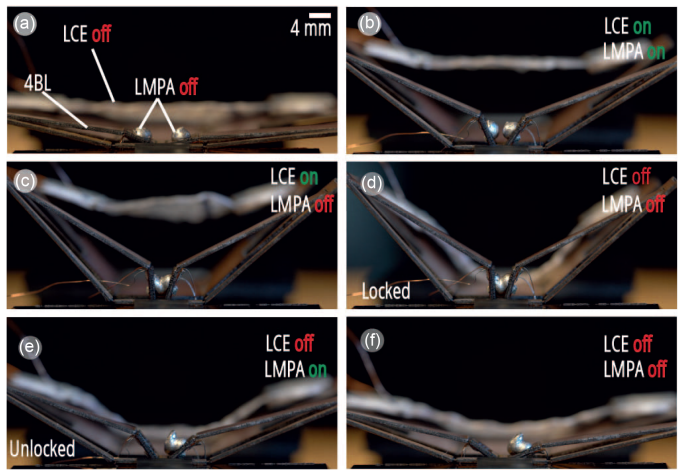

Fig. 2. Concept of the reversible self-locking mechanism with LCE, LMPA, and our conceptual mechanism design. (a) Description of our key elements to achieve self-locking apart from the folding base mechanism. (b) The LCE is activated, contracts, and pulls the mechanism to self-fold. While the LCE maintains the mechanism folded, the LMPAs on each pop-up linkage are triggered to self-fuse (i.e., melt). (c) Once the LMPAs are self-fused and cooled, the LCE is turned off, and the mechanism is locked (d). (e) To unlock our mechanism, the LMPA is triggered. (f) After unlocking, both the LMPA and the LCE are switched off.

II. DESIGN AND FABRICATION APPROACH

A. Design Principle

The fundamental design principle of Revlock is described as follows (Fig. 2). When the linear actuator is electrically activated (e.g., Joule heated), it contracts and folds the mechanism (Fig. 2(b)). Here, we chose the linear actuator liquid crystal elastomers (LCEs) due to their inherent customization features. For example, weight, easy integration with planar designs and fabrication methods, and actuation performance (e.g., actuation stress 0.4 MPa–0.8 MPa, actuation strain ~40 %, and reversibility once the stimuli cease) [23], [26], [33].

Once the origami base begins to fold, the kirigami-inspired four-bar linkages (4BL) will pop up until a programmed (estimated) position. Then, the LMPA attached to the 4BLs can

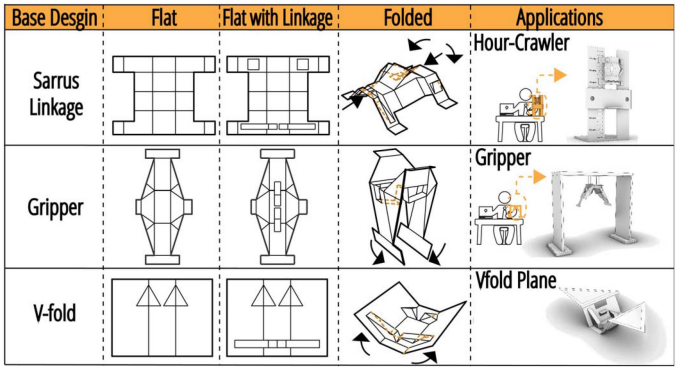

Fig. 3. Summary of the design primitives and their respective derived applications explored in their flat and folded positions, in which the black arrows indicate the folding direction.

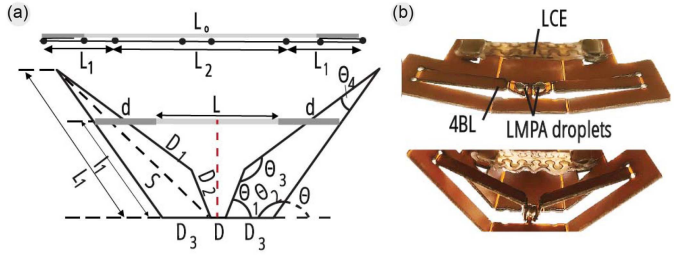

Fig. 4. Design parameters and relationships to achieve self-locking. (a) Schematic of the four-bar-linkage mechanism kinematics and geometric parameters as a function of the linear actuator strain. (b) Top-front view of the representative mechanism for reversible self-locking with the LCE, relaxed (top image), and contracted (lower image).

be controlled/triggered to change the phase of the LMPA from solid to liquid. This transition between phases is also controlled using Joule heating provided by surface mount resistors on the back of the 4BLs. After the LMPA is melted, fused and cooled back to a solid phase (Fig. 2(c)), the Joule heating of the LCE is turned off and the origami/kirigami shape is locked (Fig. 2(d)). To unlock the folded configuration of the mechanism, the LMPA is Joule heated again by the resistors. The inherent restorative force of the compliant hinges reverses the laminate composite back to its original (unfolded) shape (Fig. 2(e) and (f)). A key advantage of using origami and kirigami-inspired mechanisms is the opportunity to control multiple folds with a single input actuation [26], thus minimizing complexities related to system integration (e.g., assembly, amount of input/output requirements for actuation control with a single linear actuator). This feature is possible by selecting base designs with one degree of freedom (DOF) (i.e., its state/configuration can be defined by one independent parameter, such as angle or displacement). In this case, the base design is the 4BL shown in Figs. 2 and 4.

To validate our reversible self-locking principle, we define three reconfigurable design primitives. These three primitives are based on commonly explored origami and kirigami transmission mechanisms that use a single unidirectional actuator input [26], [27], [28]. These base designs (i.e., design primitives) are illustrated in Fig. 3 and include: i) a Sarrus linkage; ii) an Origami-inspired gripper; and iii) a V-fold base. Each base design enables different applications when combined with the LCE as a linear actuator and the LMPA for electrically controlled locking. For example, the Sarrus linkage enables reconfigurations for locomotion (e.g., crawling robot, Fig. 3, first row). The gripper naturally allows objects to be held / released (e.g., food delivery or harvesting, Fig. 3, second row). The V-fold pop-up primitive can be used as a modular element for a self-assembled glider (Fig. 3, third row, see Sup. Video for demonstration).

B. Kinematic and Dynamic Considerations for RevLock

For the RevLock approach, it is necessary to find the desired folding angle when the RevLock composite is locked (θ), Fig. 4(a). Parts of the 4BLs on the composite should be close to each other for this to happen. We can achieve a specific 4BL folding angle given the following inputs: actuation strain (ϵ) and initial length (L_o) of the linear actuator (e.g., LCE) to drive the self-folding motion. Given the desired locked angle of the 4BL (θ_1) and the lengths of the composite links d, D_2, D_3, D, L_1, and l_1, we can find the angular displacement of the self-locked 4BL (θ_2, θ_3, θ_4). By finding these outputs, we enable future sensing and feedback control opportunities with thermistors and optical sensors [29].

Furthermore, by defining the linkage length (D_2) where the LMPA droplet is located, we can find the lever arm size D_1 to assist in the self-fusing of the droplets. This design consideration also leverages small displacements of the actuator, which requires less input strength. The size of the LMPA droplets is also designed to fit the copper islands (4 mm $\times$ 3 mm $\times$ 1.5 mm) exposed on the 4BL for adherence (see Section II-D2). This sizing ensures that the fused size of the droplet is close to length D in Fig. 4(a) so that small inconsistencies in the droplet's shape or size do not impact fusing when the 4BL is folded. Given these design considerations and the kinematic relationships between the 4BL and the linear actuator, Fig. 4(a), we derived (1)–(9). The assumptions we considered were: (i) the linkages are rigid; (ii) the mechanism has ideal rotational joints; (iii) a rectilinear contraction of the LCE actuator; and (iv) a symmetric mechanism design and contraction of the LCE actuator (red dashed line).

$$\vec{L_1} + \vec{D_3} = \vec{D_1} + \vec{D_2} = \vec{S} \tag{1}$$

$$|L_2| = 2|D_3| + |D| \tag{2}$$

$$|L| = |L_o|(1 - \epsilon) \tag{3}$$

$$\theta = acos\left(\frac{\frac{|L|-|L_2|}{2} + |d|}{|l_1|}\right) \tag{4}$$

$$\theta_2 = 180 - \theta \tag{5}$$

$$|S| = \sqrt{|L_1|^2 + |D_3|^2 - 2|L_1||D_3|cos\theta_2} \tag{6}$$

$$|D_1| = |L_1| + |D_3| - |D_2| \tag{7}$$

$$\theta_3 = acos\left(\frac{|D_1|^2 + |D_2|^2 - |S|^2}{2|D_1||D_2|}\right) \tag{8}$$

$$\theta_4 = 2\pi - \theta_1 - \theta_2 - \theta_3 \tag{9}$$

To estimate the restorative torque (M) provided by the laminate flexures given a folded angle θ, we can use the sum of the

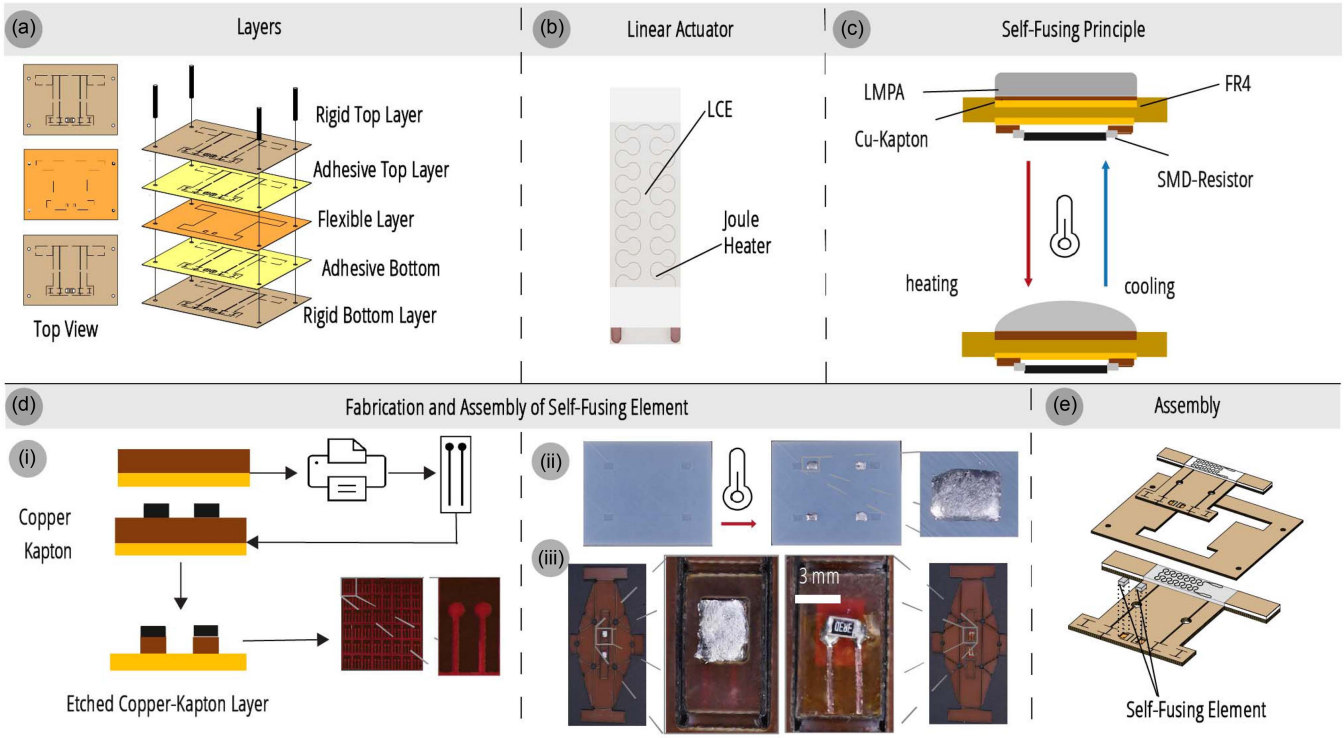

Fig. 5. Summary of the design and fabrication approach. (a) Design and fabrication of the composite layers. b) Fabrication of the liquid crystal elastomer (LCE) actuator [26]. (c) Controlling the self-fusing element with Joule heating. (d) Fabrication and assembly steps of the self-fusing elements. (i) Fabrication of the flexible layers with copper pads for the self-fusing element. (ii) Molding of the low melting point alloy for the copper pads. (iii) Assembly of the flexible circuit with the LMPA droplet on the back (left) and heating circuit on the front (right) of the composite. (e) Assembly of the composite for self-folding and locking.

potential energy stored in each flexural joint (related to torsional stiffness k_i and angle θ_i), divided by two times the folding angle θ, as described in [30].

$$M = \frac{1}{\theta}\frac{\sum_{n=i}^{N} k_i \theta_i^2}{2} \tag{10}$$

C. Timing Considerations for the Reversible Self-Locking

The timing required to fold and lock the mechanism can be controlled by the speed of actuation, the geometry of the 4BL, and the time it takes to melt and fuse the LMPA droplets. These timings depend on the kinematics of the linkages (1)–(10), geometry, and material properties of LMPA droplets [17], [31] and actuator [24], [25], [32], [33]. For instance, given the minimum heating time to reach the phase transition of LMPA, we can estimate when to trigger them during the locking motion, Fig. 6(c). To estimate this time (t), we need to consider the power input of the resistive heaters, the geometry of the droplets and the convective losses, (11) [13], [17], where m is the mass of the LMPA droplets, c is the specific heat of the LMPA, ΔT is the difference between the desired melting and ambient temperature, cl is the latent heat of the fusion coefficient for the LMPA, P is the joule heating power, h is the air heat transfer coefficient, and A is the heated surface area.

$$t = \frac{m(c\Delta T + cl)}{P - hA\Delta T}. \tag{11}$$

For the typical LMPA locking mechanisms used in this work, we estimate the minimum time required to heat from solid to liquid is approximately 14 s. However, this is likely an underestimate given that the heater is also heating additional mass (e.g., the copper traces and Kapton layers beneath the LMPA droplet) and we noticed that the LMPA creates a thin outer 'skin' that needs to break before fusing (see Supplementary Video).

D. Fabrication Approach

A key contribution in this work is the monolithic fabrication approach that integrates the linear actuator (LCE) and LMPAs into laminated origami and kirigami composites (i.e., 2D patterned layers of different materials [7], [26]). To incorporate our proposed locking mechanism without compromising weight or extra assembly steps, we leveraged the kirigami technique to create cuts and hinges, allowing the designed 4BL linkages to pop up for locking the system (Fig. 2).

Our proposed design and fabrication framework consists of the steps shown in Fig. 5. First, the cut patterns for each composite layer (e.g., rigid, flexible, adhesive, and release) were generated using an open-source tool using GrassHopper that we created as part of this work [34]. In the next step, we created the stretchable heating circuit and the LCE layer to obtain the linear actuators [26], [32], (Fig. 5(b)). Then, we prepared the self-fusing element (Fig. 5(c), Section II-D2) to integrate with the other layers for assembly (Fig. 5d). Next, we integrated the locking system (including the LCE actuator with LMPAs for timed self-locking control) for assembly and release, Fig. 5(e).

1) Fabrication of Liquid Crystal Elastomer Actuator: The LCE actuator fabrication process in this work followed

previously explored, validated, and characterized synthesis to achieve unidirectional artificial muscles [23], [24], [32], [33]. In summary, the process consisted of preparing the solution for the LCE, and casting, curing, and sandwiching the laminate sheets of LCE with the stretchable heating circuit, Fig. 5(b). To fabricate the stretchable heating circuit, we leveraged laser cut peano curved patterns (LPKF, U4 LASER) on copper tape from previous work [26], [32]. The peano curved patterns were 0.42 mm wide and 0.035 mm thick, providing a resistance of $\sim$1 Ω, and cut from off-the-shelf copper tape attached to a gel-pak substrate (Gel-Pak, delphon). For the laser cutter settings, we set the power output to 2 W, and eight passes were needed to cut the patterns of the stretchable heaters.

2) Fabrication of LMPA Reversible-Fusing Element: The LMPA (Roto144F, Field's Metal) requires a copper layer to remain attached to the mechanism. To fabricate our reversible self-locking mechanism, we used an embedded copper-coated Kapton layer (LF9120R, Pyralux) sandwiched between the rigid layers of our composite (Fig. 5(c) and (d)). To achieve flexibility in this layer for hinges while still maintaining the copper region for the LMPA, we used a solid ink printer (ColorQube 8580, Xerox) to create patternable masks for etching Fig. 5(d-i). Later, we used ferric chloride to etch away the copper except in the protected region with the solid ink mask. Next, we removed the protective mask with acetone. We utilized this process to fabricate flexible circuits for the resistor, the LMPA, and the flexible layers.

We controlled the size of the LMPA using a silicone mold (4 mm $\times$ 3 mm $\times$ 1.5 mm), Fig. 5(d-ii). Then, we added the LMPA into the mold and melted it to conform to the shape of the mold (which was based on the size of the copper islands of the mechanism). Next, once cooled and solidified, we transferred the LMPA to the surface of the embedded copper-Kapton flexible layer, Fig. 5(d-iii). To guarantee the bonding of the LMPA with the copper, we treated the copper surfaces with solder paste (B-15, Goot). Later, after assembling the composite layers (Fig. 5(e)), we heated the LMPA with a soldering iron on the copper-treated surface to ensure adherence between the metallic layers. We attached a resistor (3.3 Ω, 0805 surface mount resistor) to the backing of the flexible circuit behind the LMPA droplets for controlled heating Fig. 5(d-iii).

III. Performance of RevLock- Conceptual Design

We characterized the simplified RevLock mechanism shown in Fig. 2 for both reversibility as well as the strength of the LMPA locking. This simple mechanism uses a single LCE attached at the far end of the folding elements for folding actuation, and LMPA attached to both of the folding elements near the base for locking. To validate that the motion is reversible with locking and unlocking, we measured the folding angle and temperature of the LCE and LMPA over several cycles. A video of the folding motion was analyzed using an image analysis tool (ImageJ) and the temperatures were captured using a thermal camera (HT-19, Hti). We also measured the strength-to-weight ratio for the gripper-base mechanism in Fig. 3. Increasing weights were added until the LMPA failed to keep the grip locked in place. For all of these tests, we controlled the timing and power delivered to the actuator and locking elements using an Arduino Uno and switch circuits (IRF520 MOS Driver Module).

A. Reversibility of Self-Folding Composite With Locking

To test the reversibility of self-folding and locking of the mechanism, we actuated the mechanism through four consecutive cycles of actuation, locking, and unlocking (Fig. 6). The first cycle is the offset cycle, where the LMPA droplet from one 4BL in the mechanism is transferred to the opposing 4BL (Fig. 2(d)–(f)). This event occurs due to differences in surface energy between the LMPA and the copper island [13]. LMPAs have high surface tension (liquid) and low reactivity with metals. Thus, surface treatment of the copper pads with solder paste or flux is required before operation. We used solder paste in these experiments. We hypothesize that the interfacial energy between surfaces is sufficient to keep the bonding consistent after this offset cycle given the volume of our droplets. Although this offset cycle results in a single droplet after the first locking/unlocking cycle, using two initially separate droplets (Fig. 2(a)) is still advantageous for a composite design to naturally merge the droplets when triggered.

For each cycle, the LCE folding actuator is turned on for 150 s ($\sim$6 W, $\sim$3.3 V) and off for 130 s. For locking, the LMPA heating element is turned on for 35 s ($\sim$1.2 W, $\sim$1.7 V), 40 s after the start of LCE actuation. This heating element is turned off for 75 s to solidify the LMPA and lock the robot in place (Fig. 6(a-ii)). To unlock and reconfigure the robotic system, the LMPA heating is turned on for 20 s (to melt the LMPA) and 70 s after the LCE is turned off. The LMPA heating is then turned off for 40 s to resolidify the LMPA. We also tested an unlocking time of 12 s during the first cycle shown in Fig. 6(b)/(c). However, we found that an unlocking time of 20 s worked best for the LMPA to fully unlock in this design and that timing was used in the remaining three cycles. This is consistent with our estimate from (11). Fig. 6(b) and (c) illustrate the consistency and reversibility of our settings to trigger locking/unlocking and self-folding.

For the reversibility of our mechanism, we analyzed the folding angle and temperature for the locking/unlocking of our conceptual mechanism (Fig. 6(b)–(d)). During the first cycle, we observed an offset on the folding angle (Fig. 6(b)), which we believe is associated with residual stresses. On average, the folded and locked angle reached a peak of 41.5° $\pm$ 0.36° 220 s after the start of each cycle. Our test structure unlocked and unfolded to a minimum angle of 11.36° $\pm$ 0.36° after each cycle. This demonstrates the consistent folding control and reversibility of the RevLock approach. While only four cycles were tested in this example (still comparable to the maximum cycles from other work in Table I), LMPA has previously been demonstrated to fuse and un-fuse an average of 221 cycles [14].

We also measured the temperature of the LCE and LMPA components during each cycle. The composite self-folded for locking when the LCE reached 124.4 °C $\pm$ 1.8 °C at 75 s of each cycle, Fig. 6(c), reaching a maximum temperature of 135.5 °C $\pm$ 4 °C during the cooling of the LMPA to lock the structure. The LMPA reached a peak temperature of $\sim$88 °C when melting the LMPA sufficiently to break contact between the copper island and the LMPA, unlocking the structure between the LCE cycles. The heating of LMPA to melt shortly after the LCE cycle began was measured at 43.7 °C $\pm$ 3.2 °C, and although this measurement was consistent, we expect it to be the result of a measurement error due to measuring two nearby hotspots with the same thermal camera during the experiment (Fig. 6(d)). However, the temperature increase during this phase

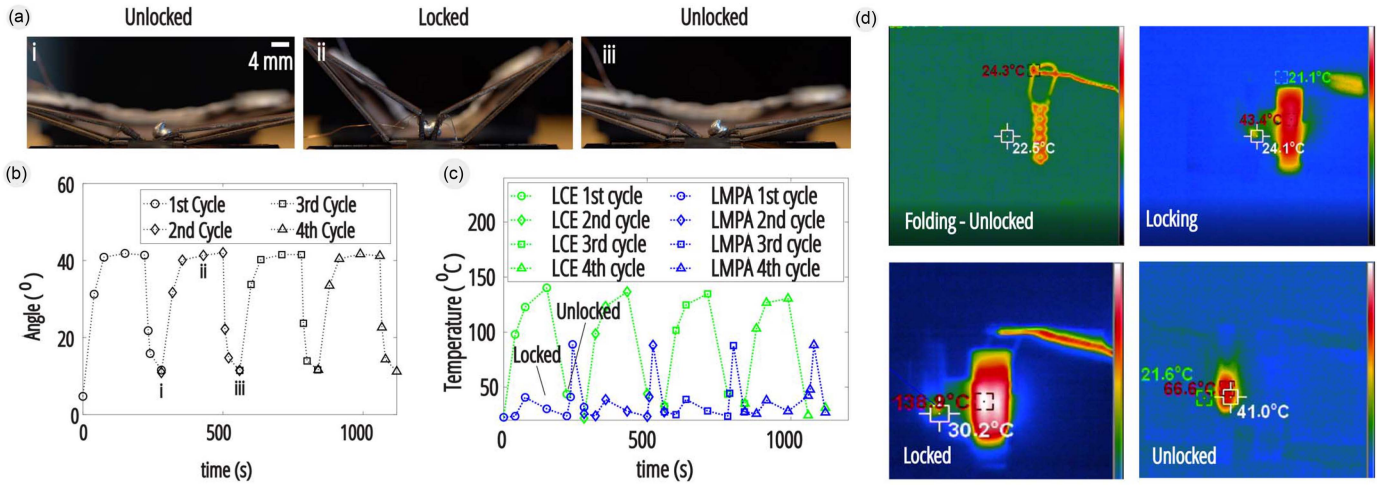

Fig. 6. Reversible self-locking performance of our conceptual design. (a) Representative photos of the locking and unlocking states of our conceptual mechanism design (i-iii) after the first cycle. (b) Reversible and repeatable self-folding motion (angle) of our mechanism controlled over time by triggering the LCE and LMPA. (c) Relationship between the LCE and LMPA temperatures for triggering reversible self-locking without constant energy input. (d) Top view of the LCE and LMPA (small heating points) when either element is Joule heated.

was sufficient to reattach the LMPA to the copper island for locking, which occurred when the LMPA cooled to 39.1 °C ± 1.2 °C).

B. Strength-to-Weight of a Self-Locking Composite

Our mechanism's concept was designed for cm-scaled applications in which load bearing is not its main usage. However, our approach can take advantage of the strength-to-weight ratio advantages of origami-inspired mechanisms [28] and the locking strength of the LMPA itself, reported to withstand a mean tensile load of 173 N using 16 separate LMPA connections) [13]. To validate this concept for our locking mechanism, we tested the gripper-inspired base design (kinematics and dynamics previously described in [28], [35]) by adding weights to pull the locked mechanism downward. The maximum strength-to-weight ratio measured for the 6.5 g locked gripper-base mechanism was 266 (1.7 kg), and failure occurred at the next weight increase at a strength-to-weight ratio of 308 (2 kg). In our case, the composite (specifically the 4BL flexure joints) failed first, so this is a conservative estimate for the locking mechanism.

IV. Demonstration of RevLock in Robotic Systems

To validate and demonstrate our framework and base designs' applicability for robotic systems, we demonstrated their usability for reversible self-locking in three separate robotic demonstrations (see video). We took advantage of their controlled and timed reconfiguration to create a crawling clock and a gripper.

A. Sarrus Linkage Base and Hour-Crawler Demo

To highlight the ability of RevLock to reconfigure into a robotic locomotion system, we demonstrated a kirigami-inspired crawling robot design using the Sarrus base primitive Fig. 7(i-ii). The robot can be deployed and locked into a crawling robot configuration from a flat and compact state. After this reconfiguration, it can achieve linear motion for locomotion, Fig. 7(i-iv).

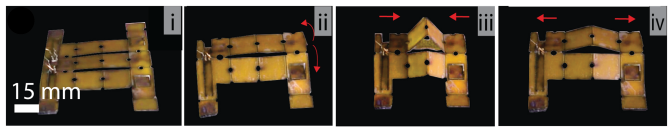

Fig. 7. Self-Assembly and motion of the Sarrus-Linkage base design. From a flat position (i), self-locked (ii), to linear motion (iii-contraction and iv-expansion).

To achieve both reconfigurations from a flat sheet and locomotion, we used two LCE actuators – one for triggering the reversible self-locking with LMPA (Fig. 7(ii)) and the second for locomotion (Fig. 7(iii)). First, the horizontal LCE contracts with the LMPA locking system, and when the LMPAs are self-fused, the mechanism is locked into its 3D crawler shape. In this configuration, the center LCE actuator controls the linear motion of the mechanism for crawling locomotion, Fig. 7(iii-iv). This deployability feature from 2D to a passively – without constant energy input – sustained 3D shape allows the system to be stored in a compact form factor and deployed when needed.

We also demonstrate integration of the robot with sensors in its environment to interact with its surroundings (Fig. 8). Our Hour-Crawler consisted of a Sarrus-based crawler magnetically attached to a fixed acrylic structure with magnetic tape, which provided a path for the robot. An ultrasonic sensor at the base of the system is connected to an Arduino Uno to detect robot proximity. Due to the asymmetric magnetic force of the magnets attached to the crawler (differential friction) and gravity, the crawler moves downward approximately 2 mm during each locomotion cycle enabled by cycling the LCE actuator. The alarm beeped within 12 cycles (each with 40 s of heating and 60 s of cooling) for this demo, moving ∼25 mm. We tested the crawler for five cycles, and within the voltages tested of 3.5 V to 4 V, the average speed was 0.02 mm/s ± 0.0036 mm/s.

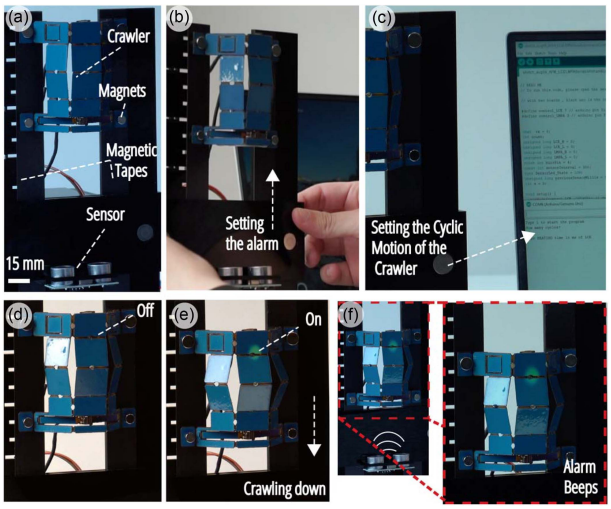

Fig. 8. Application scenario where the Sarrus base crawling robot is used as a robotic alarm clock. (a) Crawling clock and its key components. (b) Setting up the alarm according to a user's needs. (c) The user inputs the settings for the timer (e.g., LCE heating and cooling time within a cycle and its repetition). (c) Thermochromic augmented skin (i.e., layer) added to the crawler, indicating when the LCE is switching off (d) and on (e) within a cycle. (f) Alarm beeps when the crawler is near the sensor.

Fig. 9. Principle of reversible self-locking using the gripper-base. (a) Unlocked state of the gripper indicating the positions of the LMPA and LCE on the mechanism. (b) Locking position when the LCE contracts and folds the gripper to its grasping/closed position. (c) Locked gripper and d) unlocked state when the LMPA is triggered again.

B. Gripper Base and Timed Grasping Demo

Taking advantage of the reconfigurability of origami-inspired robotic gripper designs, we built a gripper based on origami-inspired forceps in [35]. This design can reconfigure into a compact shape suitable for storage in small spaces before self-folding into a grasping configuration when triggered (Fig. 9). The size of objects that can be grasped is determined by the kinematic constraints of the gripping mechanism in this design.

We attached an LCE actuator to the driving 'wings' opposite of the gripper itself in Fig. 9(a) to drive the self-folding process. This is somewhat different from the previous designs because the LCE needed to be out of the way of the 4BL mechanism with the LMPA droplets. The mechanism then uses the LCE contraction to release the 4BL for locking, Fig. 9(b). Then we activated the LMPA to lock once folded to a grasping position. When cooled, the signal to trigger the LCE is turned off and the reconfigurable gripper maintains its locking position without applied energy, Fig. 9(c). To unlock, the LMPAs can be reheated, and the restorative torque of the mechanism allows it to return to its unlocked state (Fig. 9(d)).

We demonstrated the use of this self-locking reversible robotic gripper to deliver food to fish, automate plant harvesting, and pick and place objects (Fig. 10). We triggered the LCE with an attached power supply (3.5 V and 1.5 A) for these

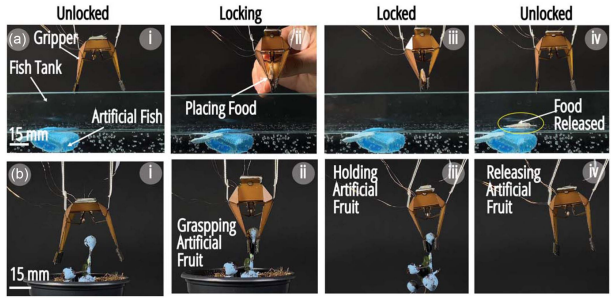

Fig. 10. Demonstration of the reversible self-locking gripper. (a) The gripper is used for delivering food to fish by reversibly self-locking (i-iv). (b) Showing the effectiveness of the gripper for fruit harvesting without requiring constant power input. It can grasp the plant, hold its position until the desired drop location, and release the fruit (i-iv).

demonstrations. For the fish demo, the LCE contracts, grasping and locking the gripper into place in 2 minutes and 50 seconds. Once the 4BLs were near each other, the LMPA heating circuit was turned on for 1 minute and 35 seconds with 1.5 V and 0.65 A. When the LMPAs are melted and diffused, their heating circuit is turned off for 2 minutes and 51 seconds to cool them down for locking. Then the LCE is turned off and the mechanism is locked. To unlock the gripper and drop the fish food, the LMPA heating circuit is turned on for 12 seconds with 1.5 V and 0.65 A. This reversibility between a locked "gripping" state (without additional power input) and an unlocked "releasing" state can be repeated as necessary.

V. Conclusion and Future Work

This letter demonstrated an approach to designing and fabricating reversible self-locking composite mechanisms that enable reconfigurable kirigami- and origami-inspired robotic systems. With RevLock, we can achieve controlled locking without constant energy input by timing the folding and popping out of our kirigami/origami mechanisms using an electrically triggered LMPA and an LCE linear actuator. We also demonstrated the use of RevLock with two robotic systems. For greater autonomy, these systems could be further integrated with sensing capabilities and augmented with different materials.

We also provided geometric and dynamic relationships to design and fabricate reversible self-locking mechanisms. Further exploration of the dynamics of origami-and kirigami-inspired composites can be used to optimize the timing of mechanism reconfiguration. For example, the compliance, self-locking parameters (e.g., sizing of copper islands and LMPA droplets), and self-locking time (11) can be optimized through mechanism design, improved modeling, and material selection. As mentioned in previous work [13] and here, the strength of the locking is highly dependent on the surface treatment between the copper pads and the LMPA droplets. So improving their bonding could also be helpful in increasing and tuning the strength of the lock.

Ultimately, RevLock enables novel designs and robotic systems for reconfiguration through self-locking and expands the toolset of methods available to the robotics community by providing: i) the capability to controllably and reversibly self-lock between configurations without constant energy input, and ii) an expanded design landscape to achieve self-reconfigurable robotic systems.

ACKNOWLEDGMENT

C. Shen and S. Paul contributed equally to this work. Also, thank you to Adrianna Stopol for her assistance during early stages of this project, and Dr. Michael Tolley from UC San Diego for initial discussions.

REFERENCES

[1] D.-Y. Lee, S.-R. Kim, J.-S. Kim, J.-J. Park, and K.-J. Cho, "Origami wheel transformer: A variable-diameter wheel drive robot using an origami structure," *Soft Robot.*, vol. 4, no. 2, pp. 163–180, 2017.

[2] S. Miyashita, S. Guitron, K. Yoshida, S. Li, D. D. Damian, and D. Rus, "Ingestible, controllable, and degradable origami robot for patching stomach wounds," in *Proc. IEEE Int. Conf. Robot. Automat.*, 2016, pp. 909–916.

[3] S. M. Felton et al., "Self-folding with shape memory composites," *Soft Matter*, vol. 9, no. 32, pp. 7688–7694, 2013.

[4] S.-J. Kim, D.-Y. Lee, G.-P. Jung, and K.-J. Cho, "An origami-inspired, self-locking robotic arm that can be folded flat," *Sci. Robot.*, vol. 3, no. 16, 2018, Art. no. eaar2915.

[5] S. Mintchev, M. Salerno, A. Cherpillod, S. Scaduto, and J. Paik, "A portable three-degrees-of-freedom force feedback origami robot for human–robot interactions," *Nature Mach. Intell.*, vol. 1, no. 12, pp. 584–593, 2019.

[6] H. Suzuki and R. J. Wood, "Origami-inspired miniature manipulator for teleoperated microsurgery," *Nature Mach. Intell.*, vol. 2, no. 8, pp. 437–446, 2020.

[7] S. Felton, M. Tolley, E. Demaine, D. Rus, and R. Wood, "A method for building self-folding machines," *Science*, vol. 345, no. 6197, pp. 644–646, 2014.

[8] M. Yim, Y. Zhang, and D. Duff, "Modular robots," *IEEE Spectr.*, vol. 39, no. 2, pp. 30–34, Feb. 2002.

[9] S. Miyashita, L. Meeker, M. T. Tolley, R. J. Wood, and D. Rus, "Self-folding miniature elastic electric devices," *Smart Mater. Struct.*, vol. 23, no. 9, 2014, Art. no. 094005.

[10] E. Hawkes et al., "Programmable matter by folding," *Proc. Nat. Acad. Sci.*, vol. 107, no. 28, pp. 12441–12445, 2010.

[11] J.-H. Na et al., "Programming reversibly self-folding origami with micropatterned photo-crosslinkable polymer trilayers," *Adv. Mater.*, vol. 27, no. 1, pp. 79–85, 2015.

[12] S.-M. Baek, S. Yim, S.-H. Chae, D.-Y. Lee, and K.-J. Cho, "Ladybird beetle–inspired compliant origami," *Sci. Robot.*, vol. 5, no. 41, 2020, Art. no. eaaz6262.

[13] J. Neubert, A. Rost, and H. Lipson, "Self-soldering connectors for modular robots," *IEEE Trans. Robot.*, vol. 30, no. 6, pp. 1344–1357, Dec. 2014.

[14] O. Testoni et al., "A 4D printed active compliant hinge for potential space applications using shape memory alloys and polymers," *Smart Mater. Structures*, vol. 30, no. 8, 2021, Art. no. 085004.

[15] K. Gilpin, A. Knaian, and D. Rus, "Robot pebbles: One centimeter modules for programmable matter through self-disassembly," in *Proc. IEEE Int. Conf. Robot. Automat.*, 2010, pp. 2485–2492.

[16] R. Niu et al., "Magnetic handshake materials as a scale-invariant platform for programmed self-assembly," *Proc. Nat. Acad. Sci.*, vol. 116, no. 49, pp. 24402–24407, 2019.

[17] A. Tonazzini, S. Mintchev, B. Schubert, B. Mazzolai, J. Shintake, and D. Floreano, "Variable stiffness fiber with self-healing capability," *Adv. Mater.*, vol. 28, no. 46, pp. 10142–10148, 2016.

[18] A. Madhukar, D. Perlitz, M. Grigola, D. Gai, and K. J. Hsia, "Bistable characteristics of thick-walled axisymmetric domes," *Int. J. Solids Structures*, vol. 51, no. 14, pp. 2590–2597, 2014.

[19] A. Brinkmeyer, M. Santer, A. Pirrera, and P. Weaver, "Pseudo-bistable self-actuated domes for morphing applications," *Int. J. Solids Structures*, vol. 49, no. 9, pp. 1077–1087, 2012.

[20] L. Yao, R. Niiyama, J. Ou, S. Follmer, C. Della Silva, and H. Ishii, "PneUI: Pneumatically actuated soft composite materials for shape changing interfaces," in *Proc. 26th Annu. ACM Symp. User Interface Softw. Technol.*, 2013, pp. 13–22.

[21] D. Rus and M. T. Tolley, "Design, fabrication and control of soft robots," *Nature*, vol. 521, no. 7553, pp. 467–475, 2015.

[22] H. Liu et al., "Shape-programmable, deformation-locking, and self-sensing artificial muscle based on liquid crystal elastomer and low–melting point alloy," *Sci. Adv.*, vol. 8, no. 20, 2022, Art. no. eabn5722.

[23] C. Yakacki, M. Saed, D. Nair, T. Gong, S. Reed, and C. Bowman, "Tailorable and programmable liquid-crystalline elastomers using a two-stage thiol–acrylate reaction," *RSC Adv.*, vol. 5, no. 25, pp. 18997–19001, 2015.

[24] A. Minori, S. Jadhav, Q. He, S. Cai, and M. Tolley, "Reversible actuation of origami inspired composites using liquid crystal elastomers," in *Proc. Smart Mater., Adaptive Structures Intell. Syst.*, 2017, Art. no. V001T08A015.

[25] Q. He, Z. Wang, Z. Song, and S. Cai, "Bioinspired design of vascular artificial muscle," *Adv. Mater. Technol.*, vol. 4, no. 1, 2019, Art. no. 1800244.

[26] A. F. Minori et al., "Reversible actuation for self-folding modular machines using liquid crystal elastomer," *Smart Mater. Structures*, vol. 29, no. 10, 2020, Art. no. 105003.

[27] B. G. Winder, S. P. Magleby, and L. L. Howell, "Kinematic representations of pop-up paper mechanisms," *J. Mechanisms Robot.*, vol. 1, p. 021009, 2009, doi: 10.1115/1.3046128.

[28] E. W. Wilcox et al., "Considering mechanical advantage in the design and actuation of an origami-based mechanism," in *Proc. Int. Des. Eng. Tech. Conf.s Comput. Inf. Eng. Conf.*, 2015, Art. no. V05BT08A055.

[29] M. E. W. Nisser, S. M. Felton, M. T. Tolley, M. Rubenstein, and R. J. Wood, "Feedback-controlled self-folding of autonomous robot collectives," in *Proc. IEEE/RSJ Int. Conf. Intell. Robots Syst.*, 2016, pp. 1254–1261.

[30] R. J. Wood, S. Avadhanula, R. Sahai, E. Steltz, and R. S. Fearing, "Microrobot design using fiber reinforced composites," *J. Mechan. Des.*, vol. 130, p. 052304, 2008, doi: 10.1115/1.2885509.

[31] W. Shan, T. Lu, Z. Wang, and C. Majidi, "Thermal analysis and design of a multi-layered rigidity tunable composite," *Int. J. Heat Mass Transfer*, vol. 66, pp. 271–278, 2013.

[32] A. F. Minori, S. Jadhav, H. Chen, S. Fong, and M. T. Tolley, "Power amplification for jumping soft robots actuated by artificial muscles," *Front. Robot. AI*, vol. 9, 2022, Art. no. 844282.

[33] Q. He, Z. Wang, Y. Wang, A. Minori, M. T. Tolley, and S. Cai, "Electrically controlled liquid crystal elastomer–based soft tubular actuator with multimodal actuation," *Sci. Adv.*, vol. 5, no. 10, 2019, Art. no. eaax5746.

[34] A. Fernandes Minori et al., "RevLock-Layer generator," Apr. 2023, Accessed: Feb. 18, 2023. [Online]. Available: https://github.com/AFMinad/tutorial_code_vid_rlock.git

[35] B. J. Edmondson, L. A. Bowen, C. L. Grames, S. P. Magleby, L. L. Howell, and T. C. Bateman, "Oriceps: Origami-inspired forceps," in *Proc. Smart Mater., Adaptive Struct. Intell. Syst.*, 2013, Art. no. V001T01A027.